Journal of Extracellular Biology

RESEARCH ARTICLE OPEN ACCESS

Revisiting the Nanoflow Cytometric Quantification of Extracellular Vesicles Under the Framework of ICH Q14 Guidelines

Ganghui Li[1] | Qizhe Cai[2] | Yanan Dong[3] | Xiang Li[4] | Xi Qin[4] | Miaomiao Xue[3] | Haifeng Song[5] | Yi Wang[3,6]

[1]China Pharmaceutical University, Nanjing, China | [2]Department of Ultrasound, Beijing Chao-Yang Hospital, Capital Medical University, Beijing, China | [3]PanExo Biotech Co Ltd., Beijing, China | [4]National Institutes for Food and Drug Control, Beijing, China | [5]State Key Laboratory of Proteomics, Beijing Proteome Research Center, National Center for Protein Sciences (Beijing), Beijing Institute of Lifeomics, Beijing, China | [6]Guangxi Key Laboratory of Bioactive Molecules Research and Evaluation, Guangxi, China

Correspondence: Haifeng Song (songhf@vip.163.com) | Yi Wang (wangy@panexobio.com)

Received: 23 November 2024 | **Revised:** 14 March 2025 | **Accepted:** 26 March 2025

Funding: This work was supported by Ministry of Science and Technology (China) grant (2015ZX09501008-006, 2015ZX09501007-002-05), National Science Foundation of China grant (81272701/H1617, 31400733) and Guangxi Key Laboratory of Bioactive Molecules Research and Evaluation grant (BMRE-2022-KF02).

Keywords: extracellular vesicles | ICH Q14 | methodological validation | particle concentration detection

ABSTRACT

Nanoflow cytometry (nanoFCM) is an increasingly important analytical procedure in every aspect of extracellular vesicle (EV) research, particularly in the development of EV-based therapeutics. The main objective of this study was to evaluate and optimise the key determinant factors of nanoFCM in the quantification analysis of EVs to ensure its consistency and reliability in the development of EV therapeutic drugs, thereby serving as a potential quality control measure. Our investigation followed the International Council for Harmonisation of Technical Requirements for Pharmaceuticals for Human Use (ICH) Q14 guideline. We revisited the day-to-day practice of nanoFCM measurement for HEK293 cell-derived and milk-derived EVs (mEVs), focusing on optimising particle quantification and identifying risk factors. Initial evaluation of the procedure revealed a considerable lack of consistency and reliability, which was then subjected to extensive optimisation. The key outcomes of this study include: (1) an optimised analytic procedure incorporating Tween-20, which significantly enhanced the precision and accuracy of the nanoFCM measurement and expanded the reportable range; (2) an analytical target profile (ATP) which provides a preliminary standard for future validation of nanoFCM procedures. Overall, this study serves as a foundation for future efforts towards the standardisation of analytical procedures for EV therapeutics.

1 | Introduction

Analytical procedures constitute an essential component of translational research and development of extracellular vesicle (EV)-based therapeutics. Although previous proof-of-concept studies and the minimal information for studies of EVs (MISEV2023) guidelines provided a basic framework for the characterisation and analysis of EV samples, analytical procedures described in these references are, however, distinct from those used in pharmaceutical development. A lack of harmonised analytical procedure systems in the EV field hampered the translation of EV therapeutics from laboratory to industrial and clinical applications.

Ganghui Li and Qizhe Cai contributed equally to this work.

The International Council for Harmonisation of Technical Requirements for Pharmaceuticals for Human Use (ICH) recently published a guideline for the development of analytical procedures, ICH Q14 (Q14 2023), which provided a systematic framework for the development of analytical procedures that can be adopted as quality control measures in the future: towards a preset target profile, a series of risk factor analyses and optimisation could significantly improve the robustness and reliability of the analytical procedure. It is particularly valuable for emerging therapeutic paradigms like EV, where there is a systemic lack of robust and dedicated analytical methodologies.

Reliable and consistent measurement of EV particle number is the foundation of EV analysis. Nanoflow cytometry (nanoFCM) is a versatile platform widely used for quantifying EV particles, measuring size distribution and identifying EV surface proteins (Tian et al. 2020). In an attempt to implement the ICH Q14 in the development of analytical procedures for EV therapeutics, we revisited nanoFCM and optimised its operating procedures for HEK293 cell-derived EVs (hEVs) and bovine milk-derived EVs (mEVs) under the ICH Q14 framework. Existing literature (Arab et al. 2021; Leung et al. 2024; Mladenovic et al. 2024; Yim et al. 2023) and experience from daily practice at our company all showed that the precision of particle quantification (gauged as CV%) using nanoFCM varies from 10% to 30%. A number of known risk factors influence the reliability of the measurement. Despite its widespread adoption, it remains unclear whether the commonly practiced procedure for nanoFCM meets the requirements of a viable analytical method for determining the arguably most important quality attribute: particle number. There is a clear need to systematically assess and potentially optimise the operating procedure of nanoFCM. The outcome of this study includes several organised tables and diagrams for nanoFCM: (1) an analytical target profile (ATP), (2) an Ishikawa diagram and a list of risk factors, (3) a detailed procedure description to ensure the consistent and reliable execution of nanoFCM analysis as a potential quality control measure.

2 | Methods and Material

2.1 | Cell Culture and Preparation of the hEVs and Cell Debris

Human HEK293F cells were cultured in 7.5% CO_2 using a CD05 medium (OPM; 81070-001) in Corning flasks. After 72 h, the viability of the cells was above 93%, and the concentration reached 2.2×10^6 cells/mL.

To prepare the hEVs, 600 mL supernatant was centrifuged at 3500 rpm for 60 min at 4°C, then filtered through a 0.45 μm membrane. The filtrate was concentrated by a hollow fibre tangential-flow filtration (TFF) column with a 300 kDa MWCO to 1/20 of its original volume, with the OD_{280} dropping below 0.02 AU. This crude EV suspension was further purified using a 20 mL Capto Core 700 BE-SEC column on an Akta-Pure protein purification system (Cytiva, AKTA Pure25 M1), with a flow rate at 3 mL/min using PBS as the mobile phase. The hEVs were collected at the void volume with a UV absorbance ratio of A260/A280 between 1.0 and 1.2. The collected sample was then subjected to density gradient ultracentrifugation (DGUC) (details provided below) as the final step of purification, and the preparation obtained was used as the stock solution of hEVs.

To prepare cell debris, 3×10^6 HEK293F cells were collected and centrifuged at 1500 rpm for 10 min. The supernatant was discarded, and the cell pellet was resuspended in 1 mL PBS. This process was repeated once. The pelleted cells were then lysed by sonication for 10 min, and the lysate was filtered through a 0.45 μm membrane to collect the cell debris. Subsequently, 1% Tween-20 was added to the cell debris, ensuring that the final concentration of Tween-20 reached 0.03% before being used as particulate impurity samples.

2.2 | Preparation of mEVs and Milk Fat Globule Membrane (MFGM)

The mEVs were purified following the steps established previously (Xu et al. 2022). In brief, whey solution prepared by sodium phosphate precipitation of skim milk was consecutively processed using TFF, Capto Core 700 BE-SEC column and DGUC. From a total of 13 density layers from DGUC, layers 9–11 were combined and used as the mEV stock solution. The top layer from the DGUC procedure was collected and filtered through a 0.45 μm membrane, to which 1% Tween-20 was added to a final Tween-20 concentration at 0.03%, and the MFGM suspension was ready to use.

2.3 | Preparation of Casein Micelles

To prepare casein micelles, 200 mg of casein powder (Sigma; C5890) was dissolved in 2 mL 0.1 M NaOH and heated at 100°C for 20 min (Sadiq et al. 2021). After complete dissolution, preheated 5× PBS was slowly added, and the solution was then allowed to cool to room temperature (RT). The mixture was filtered through a 0.45 μm membrane, to which 1% Tween-20 was added to ensure a final concentration of Tween-20 at 0.03%, and the casein micelle suspension was ready to use in the following studies. The characterisation results of MFGM and casein micelles are shown in Figure S1.

2.4 | Preparation of Large Fragment DNA

A plasmid containing the EGFP sequence was used, purchased from Addgene (catalogue number #80605), with a total length of 5279 bp. The characterisation results of cell debris and large fragment DNA are shown in Figure S2.

2.5 | NanoFCM

EV particles were measured using a Flow Nano Analyzer (NanoFCM Inc., N30E) equipped with a 488 nm laser pre-calibrated with 250 nm silica nanospheres and a set of silica nanosphere cocktails of 68, 91, 113 and 155 nm (NanoFCM Inc.).

EV samples were diluted with 1× DPBS (137 mM NaCl, 0.9 mM $CaCl_2$, 0.5 mM $MgCl_2$, 1.47 mM KH_2PO_4, 8.06 mM Na_2HPO_4 and 2.7 mM KCl), with or without 0.03% Tween-20, to the proper concentration before directly undergoing nanoFCM analysis without antibody or due staining. The data was acquired under standardised conditions of 10 mW laser power, 10% SS decay and 1 kPa sampling pressure with the blank DPBS as a negative control. EV concentration and size distribution were calculated using the nFCM software (NanoFCM Profession V2.31).

For particle size estimation, a gate of 40–200 nm was applied, encompassing > 99% of the detected particles. Particle concentration values were converted to particles per mL of the starting material using the software's analytical algorithms. All measurements were performed in triplicate to ensure reproducibility.

2.6 | Protein Quantification in EV

The EV samples were lysed using a lysis buffer (Beyotime Biotechnology, P0013B), and protein quantification was performed using a Bicinchoninic Acid (BCA) Protein Assay Kit (Beyotime Biotechnology, P00010) according to the manufacturer's instructions, with BSA as the standard protein reference.

2.7 | DGUC

To perform DGUC, an iodixanol gradient, consisting of 40%, 20%, 10% and 5%, each 4 mL, was prepared in a 20 mL open top polyallomer tube (Thermo Fisher, 75000610) by mixing 60% (w/v) aqueous iodixanol solution (Axis-Shield, 1114542-1) with a buffer containing 0.25 M sucrose, 6 mM EDTA and 60 mM Tris-HCl (pH 7.4). The EV preparation was overlaid on the top, and the tube was centrifuged for 18 h at 4°C, 110,000 × *g* using a S50-A Ti Rotor (Beckman) in a Thermo Sorvall MTX150 Microcentrifuge (Beckman). The gradient fractions (1.5 mL each) were collected from top to bottom for further analysis.

To estimate the density of each fraction, a standard curve was prepared using the aforementioned iodixanol gradient solutions with a 1:200 dilution in the same 0.25 M sucrose buffer. UV absorbance was measured at 310 nm.

2.8 | Transmission Electron Microscopy (TEM)

To determine the morphology of hEVs and mEVs, the EVs samples (10 μL each) were dropped onto formvar carbon-coated copper grids, stained with 10 μL of 3% phosphotungstic acid for 3 min and fixed with 2% glutaraldehyde for 5 min. After the samples were dried, TEM was performed with a JEM-2100 system (Jeol Ltd, Tokyo, Japan) at 200 kV.

2.9 | Precision and Linearity Analysis

High-concentration stock solutions of hEVs and mEVs were centrifuged at 16,000 × *g* for 40 min at 4°C. The supernatant of each preparation was collected and diluted with DPBS or DPBS containing 0.03% Tween-20 to levels appropriate for measurement using nanoFCM. The concentrations of the initial stock solutions were determined to be 2×10^{13} for mEV and 4×10^{11} p/mL for hEV. A series of 10-fold dilutions were performed with DPBS or DPBS containing 0.03% Tween-20, generating concentrations that covered six orders of magnitude (2×10^{13}–2×10^{8} p/mL) for mEV and four orders of magnitude (4×10^{11}–4×10^{8} p/mL) for hEV. Each concentration level was prepared in six replicates (Figure S3). Each sample was then diluted to the appropriate concentration to be quantified by nanoFCM. The data were compiled and statistically analysed.

2.10 | Accuracy and Reportable Range Analysis Procedure

The stock solutions of mEVs and hEVs were pre-diluted to 8×10^{8} p/mL to ensure that approximately 17,000 particles were captured by nanoFCM within 60 s. They were then subjected to a two-fold serial dilution using either DPBS or DPBS containing 0.03% Tween-20, with each sample prepared in six replicates. The particle concentration of each sample was measured using nanoFCM, and the data were analysed statistically (Figure S4).

2.11 | Risk Factor – Containers

The stock solutions of mEVs and hEVs were pre-diluted to approximately 1.5×10^{9} p/mL using DPBS, divided into 8 aliquots (100 μL each) and placed into 4 types of containers in duplicates (glass tube, PCR tube, standard Eppendorf tube and protein low-binding Eppendorf tube). Four tubes (Tube_1 to Tube_4) were incubated at RT for 2 h, whilst the other four (Tube_5 to Tube_8) were incubated at 4°C for 2 h. Subsequently, all samples were diluted 5-fold and analysed using nanoFCM.

2.12 | Risk Factor – Pipette Tips

The stock solutions of mEVs and hEVs in DPBS were transferred to a glass tube (Tube-1) using either standard or low-binding pipette tips (KG1212 and KG1233-L, respectively, Kirgen). The particle concentration was measured using nanoFCM. This suspension was then sequentially transferred from Tube-1 to Tube-5, with the particle concentrations measured in each tube. The sampling and the measurement were repeated six times at each stage (Figure S5).

2.13 | Risk Factor – Sampling Volume

The stock solution of mEVs was centrifuged at 16,000 × *g* and 4°C for 10 min, then the supernatant was pre-diluted to approximately 1.5×10^{13} p/mL using DPBS containing 0.03% Tween-20. The solution was divided into 3 aliquots (500 μL each), which were placed into three low-protein-binding Eppendorf tubes (labelled as Tube-1, Tube-2 and Tube-3). Using low-binding pipette tips, 10, 20 and 50 μL of mEVs were transferred from Tube-1, Tube-

2 and Tube-3 into low-binding Eppendorf tubes containing 90, 180 and 450 μL of DPBS with 0.03% Tween-20, respectively, each with 6 replicates. These samples were further diluted with DPBS containing Tween-20 to the proper concentration for nanoFCM analysis (Figure S6).

2.14 | Risk Factor – Diluting Reagents

Seven diluting reagents were prepared with DPBS buffer: sucrose (Aladdin; S112231), Triton X-100 (Solarbio; T8200), Tween-20 (Solarbio; T8220), Tween-80 (Solarbio; T8360), glycerol (Aladdin; G116203) and SDS (Aladdin; S108346).

The stock solutions of mEVs and hEVs were pre-diluted with DPBS to concentrations of 1×10^{13} and 4×10^{10} p/mL, respectively, and mixed with the dispersant solutions so that the final concentrations are matching the following: sucrose (0.03%, 0.1%, 0.3%, 1%, 3%, w/v); Triton X-100 (0.01%, 0.025%, 0.05%, 0.1%, 0.25%, w/v); Tween-20 (0.001%, 0.01%, 0.1%, 0.5%, 1%, w/v); Tween-80 (0.03%, 0.05%, 0.1%, 0.25%, 0.5%, w/v); glycerol (0.02%, 0.1%, 0.5%, 2.5%, 10%, v/v); and SDS (0.00025%, 0.001%, 0.0025%, 0.01%, 0.025%, w/v). After vortexing for 10 s, the samples were incubated at RT for 30 min and then centrifuged at 4°C, 16,000 × *g* for 40 min. The supernatant was diluted to a concentration range of 1.5×10^8–6.0×10^8 p/mL using the same dispersant containing diluent solutions for nanoFCM analysis. These procedures, including the dilution process and nanoFCM data acquisition, were repeated six times (Figure 7a).

To further evaluate the effects of Tween-20, concentrations of 0.001%, 0.003%, 0.01%, 0.03%, 0.1% and 0.5% were included in the diluent. These solutions were handled and analysed in the same manner as described above. The process was repeated six times.

2.15 | Robustness – Non-Particulate Impurities

Four non-particulate solutions were evaluated in this study. Three proteins, carbonic anhydrase, aldolase and thyroglobulin (all from GE Healthcare 28-4038-42), were dissolved in DPBS containing 0.03% Tween-20 and serial diluted to 8 mg/mL, 800 μg/m, 80 μg/mL, 8 μg/mL, 800 ng/mL and 80 ng/mL. Total RNA was extracted from HEK293F cells following the user instruction (QIAGEN GmbH), quantified by Nanodrop and diluted to 400 μg/mL, 40 μg/mL, 4 μg/mL, 400 ng/mL, 40 ng/mL and 4 ng/Ml with DPBS containing 0.03% Tween-20.

Each impurity sample solution was 1:1 mixed with mEVs and hEVs pre-diluted with DPBS containing 0.03% Tween-20 to 8×10^8 p/mL, vortexed for 10 s and centrifuged at 16,000 × *g* for 40 min. The supernatant was analysed using nanoFCM. These procedures were repeated six times (Figure S7).

2.16 | Robustness – Particulate Impurities

Four particulate impurities were evaluated in this study. MFGM and casein micelles were suspended in DPBS containing 0.03% Tween-20 and diluted to 4×10^{11}, 4×10^{10}, 4×10^9, 4×10^8, 4×10^7 and 4×10^6 p/mL. HEK293F cell debris were similarly suspended in DPBS containing 0.03% Tween-20 and diluted to 4×10^{10}, 4×10^9, 4×10^8, 4×10^7 and 4×10^6 p/mL. Large circular plasmid DNA was suspended in DPBS containing 0.03% Tween-20 and diluted to 1 mg/mL, 100 μg/mL, 10 μg/mL, 1 μg/mL, 100 ng/mL and 10 ng/mL.

The mEV stock solution was pre-diluted using DPBS containing 0.03% Tween-20 to 2 concentrations 4×10^{11} and 4×10^8 p/mL, which were separately 1:1 mixed with MFGM and casein micelles at concentrations ranging from 4×10^{11} to 4×10^9 and 4×10^8 to 4×10^6 p/mL, respectively. After proper dilution with the Tween-20-containing DPBS buffer, the EV samples were analysed by nanoFCM. These processes were repeated six times (Figure S8).

The hEV stock solution was pre-diluted to 4×10^{10} and 4×10^8 p/mL using DPBS containing 0.03% Tween-20. The high and low concentration samples were 1:1 mixed with HEK293F cell debris at 4×10^{10}–4×10^8 and 4×10^8–4×10^6 p/mL, respectively. The low concentration hEVs sample (8×10^8 p/mL) was 1:1 mixed with DNA fragments at 1.73×10^6, 3.04×10^6, 4.94×10^6, 2.38×10^7, 2.06×10^8 and 1.53×10^9 p/mL, respectively. Then, the mixture was diluted with Tween-20-containing DPBS to the proper concentration and analysed by nanoFCM. These processes were repeated six times (Figure S9), and the results were similarly analysed.

2.17 | Statistical Analysis

Data plotting and statistical analyses were performed using R. Data are presented as mean ± standard deviation (SD)

3 | Results

3.1 | ATP

According to ICH Q14, the ATP of a pharmaceutical product consists of the following four attributes:

Intended purpose

To quantify the number of EV particles in a given volume within a given sample, thereby deducing the particle concentration in this sample.

Link to CQA

The number (concentration) of EV particles is a prerequisite for a number of critical procedures in the manufacturing process: (1) API loading; (2) filling amount in the final formulation. The number of particles is a vital factor for the delivery capacity of the final formulation, which predicates safety and efficacy.

Characteristics of the reportable results

Performance characteristics	Acceptance criteria	Rationale
Accuracy	$-10.0\% \leq$ deviation from theoretical particle number $\leq 10.0\%$	Due to an absence of well recognised standard EV particles with robustly quantified particle number, and a lack of correlation among various particle quantification methods, we adopted an accuracy measure commonly utilised for biotherapeutics, supplemented with an arbitrary criteria of ±10%: within the range of particle concentration recommended by the manufacture, a series of sequential two-fold dilution should lead to measured particle concentration within 90%–110% of expected (theoretical) value.
Precision	RSD < 10%	
Robustness	Non-particulate impurities: RNA and protein Particulate impurities: MFGM Casein micelle Cellular debris Large DNA fragments	Evaluation of robustness comprised of two categories, the tolerance of (a) non-particulate impurities and (b) particulate impurities (e.g., MFGM, casein micelle, cellular debris, DNA fragment) during measurement.
Reportable range	LLOQ, ULOQ, LOD: TBD	The allowed range of particle concentrations recommended by the manufacturer is 1×10^7–1×10^9 p/mL. With proper dilution, this technology should be able to quantify EV samples with a concentration as high as 5×10^{13} p/mL (currently achievable upper limit of mEV concentration in this study). The LOD was set based upon the discernibility of the signal from baseline noises obtained from PBS or ultrapure water.

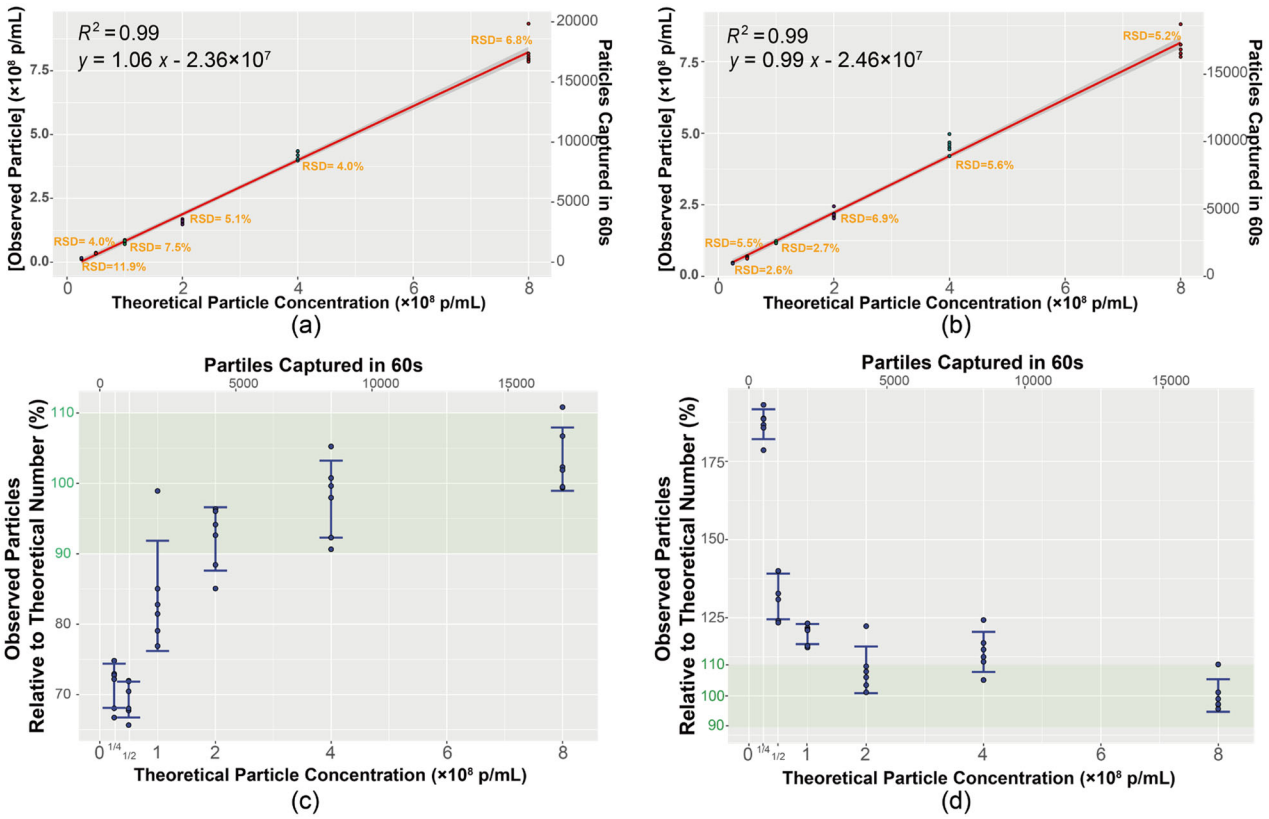

FIGURE 1 | Accuracy of nanoFCM detection for mEVs and hEVs in a serial 2-fold dilution with DPBS. (a and b) Regression curves of observed versus theoretical particle concentrations for mEVs and hEVs, respectively. The starting theoretical concentration was 8×10^8 p/mL, with every dilution repeated six times. Shown in the chart are the RSD value of the six replicates at each theoretical concentration, and the equation and the R^2 from the linear regression. The particle numbers captured in 60 s by nanoFCM corresponding to the observed particle are also shown in the y-axis to the right. (c and d) Percentage of the observed particle concentration relative to the theoretical particle concentration at each theoretical particle concentration for mEVs and hEVs, respectively. The range between 90% and 110% was highlighted in green. The blue error bars represent the standard deviation of six replicates at each theoretical concentration. The particle numbers captured in 60 s by nanoFCM were also shown in the x-axis on the top.

3.2 | Evaluation of the ATP Characteristics Without Optimisation of Methodology

3.2.1 | Accuracy

For a biotherapeutic entity without a validated standard (e.g., EV), the quantification of serially diluted samples was often adopted for evaluating analytical accuracy. Based on the range of particle concentration recommended by the manufacturer, the number of particles captured in 60 s is ideally between 500 and 17,000, corresponding to 2.5×10^7–8×10^8 p/mL. We carried out serial two-fold dilution of the mEV and hEV samples. The linearity of the serial dilution appeared to be satisfactory (Figure 1a,b); however, the 10^7 intercept on the Y-axis suggested significant deviations from theoretical values. The deviation is more clearly illustrated in Figure 1c,d, where the acceptable accuracy range (deviation no greater than 10%) for mEV was between 4×10^8 and 8×10^8 p/mL, whilst none of the diluted data points fell within the acceptable accuracy range for HEK293 EV. A notable observation from the results in Figure 1 was that the accuracy of measurement deteriorated in opposite directions for mEV and hEV. That is, nanoFCM tended to produce 'underestimated' results for mEV whilst overestimating the particle concentrations of hEV samples. Significant methodology optimisation is thus needed to improve the accuracy of the measurement.

3.2.2 | Precision and Reportable Range

We evaluated the precision of nanoFCM measurement across a large range of particle concentrations. As described above, samples with particle concentration greater than 10^9 p/mL have to be diluted to reach the recommended range (2.5×10^7–8×10^8 p/mL). Consequently, samples with higher concentrations would undergo more intensive dilution. This assay can, therefore, help determine how dilution affected the precision of the measurement and explore the reportable range of the instrument. For the highest concentration samples, we selected those achievable in our laboratory (mEV: 3×10^{13} p/mL, hEV: 2×10^{12} p/mL). For the lowest concentration samples, we used those that did not require further dilution (i.e., 10^8 p/mL). The experiment design was depicted in Figure S1: a series of samples with concentrations ranging from 2×10^8 to 2×10^{13} p/mL was prepared to represent the various samples obtained from daily R&D and manufacturing processes. Each of these samples was aliquoted into six vials and diluted accordingly to 2×10^8 p/Ml, respectively, prior to nanoFCM analysis. The slope, Y-intercept and linearity (gauged by R^2) were used to reflect the precision of measurements.

The slopes for both mEV and hEV were greater than 1.1, indicating that the measured particle concentrations deviated by more than 10% from the expected values. The Y-intercepts were

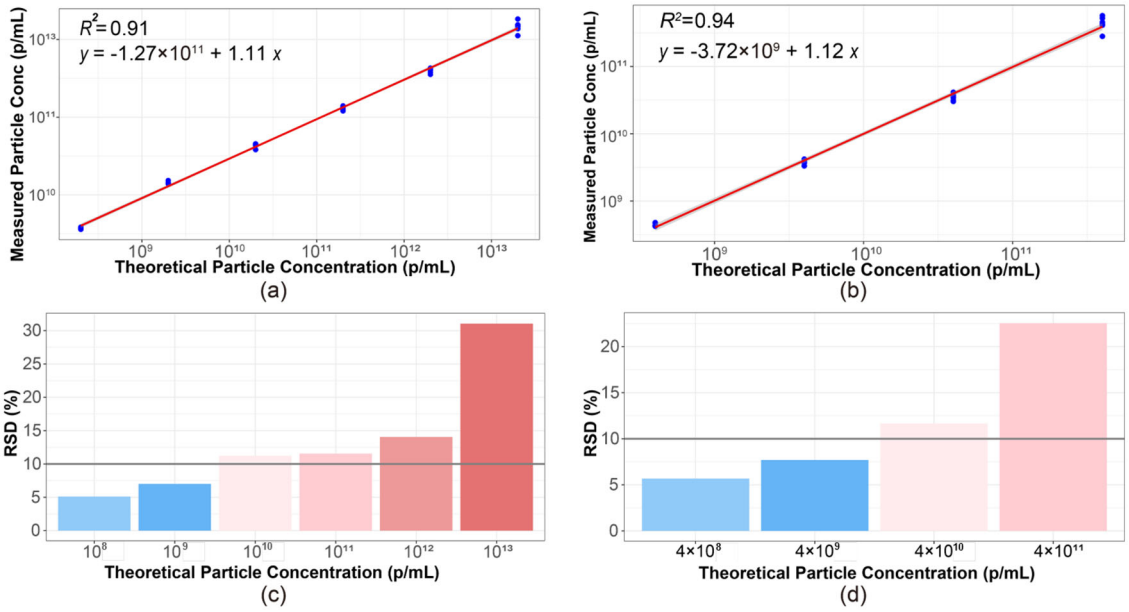

FIGURE 2 | Precision of nanoFCM detection for mEVs and hEVs in a serial 10-fold dilution with DPBS. (a and b) Regression curves of observed over theoretical particle concentrations for mEVs and hEVs, respectively. The starting theoretical concentrations for mEVs and hEVs were 2×10^{13} and 4×10^{11} p/mL, respectively. Each dilution was performed in six replicates. The regression equation and the R^2 were also shown in the charts. (c and d) RSD values of the six replicates at each theoretical particle concentration for mEVs and hEVs. The 10% threshold was indicated as a grey line.

on the orders of 10^{11} and 10^9 for mEV and hEV, respectively, whilst the R^2 values were only slightly above 0.9 (Figure 2a,b). Most importantly, the results highlighted a significant dependence of relative standard deviation (RSD) on the folds of dilution. For samples with concentrations of 2×10^{10} p/mL or higher, the precision was no longer acceptable, with RSD above 10%. For routine triplicate measurement commonly practised, one should not rely too heavily on the results from highly concentrated samples. By combining the results from Figures 1 and 2, we determined that the reportable range with acceptable precision (RSD $\leq$ 10%), without optimisation of methods, was between 4×10^8 and 4×10^9 p/mL for both mEV and hEV. This finding underscores the need for comprehensive optimisations.

3.3 | Ishikawa Diagram and Optimisation of Risk Factors

For a pragmatic approach of revealing the contributing factors for the large variations during measurement, we followed the recommendations in ICH Q14 and created an Ishikawa diagram for nanoFCM measurements to identify potential risk factors for evaluation and optimisation (Figure 3). Sample handling emerged as the single most critical factor for nanoFCM, as it appeared in five out of six major categories of the risk factor analysis, which were then sequentially investigated.

3.3.1 | Material-Containers

We evaluated four different types of containers for sample processing at RT and 4°C, using an EV sample with a particle concentration determined just before the assay. The concentration ranged from 2.5×10^7 to 8×10^8 p/mL. Overall, the particle concentration of EVs after storage tended to increase, causing significant deviations from the theoretical particle concentration. It seems to suggest that the dissolution of particulate impurities from the containers is a primary cause of this distortion. Glass vials and qPCR tubes showed the best performance for mEV, with low RSD and minimal deviation from theoretical values, as well as insensitivity to temperature (Figure 4a). EVs of HEK293 cells appeared to be more temperature-sensitive than mEV and should be handled at 4°C (Figure 4b). Both low adsorption Eppendorf tubes and glass vials worked well for storage. In general, glass vials should be the primary choice of container for handling EV samples during nanoFCM measurement.

3.3.2 | Material-Pipette Tips

We next compared the performance of ordinary pipette tips and low adsorption pipette tips during five consecutive transfers of EV solutions from one glass vial to another. Results were normalised based on the particle concentration of the original sample, with 100% indicating an exact match between the transferred sample and the original. Regarding the precision of the measurement (i.e., RSD), neither type of tip consistently provided satisfactory performance. However, ordinary tips exhibited narrower variations in more cases (Figure 5a,b). For accuracy, namely the average from each batch of six samples, low adsorption tips performed better than ordinary tips. Overall, low adsorption pipette tips are slightly preferable for handling EV samples during nanoFCM measurements.

3.3.3 | Process – Sampling Volume

For mEV samples with elevated concentrations (> 10^{12} p/mL), the increase in viscosity becomes noticeable as concentration increases. We evaluated the impact of viscosity on the precision

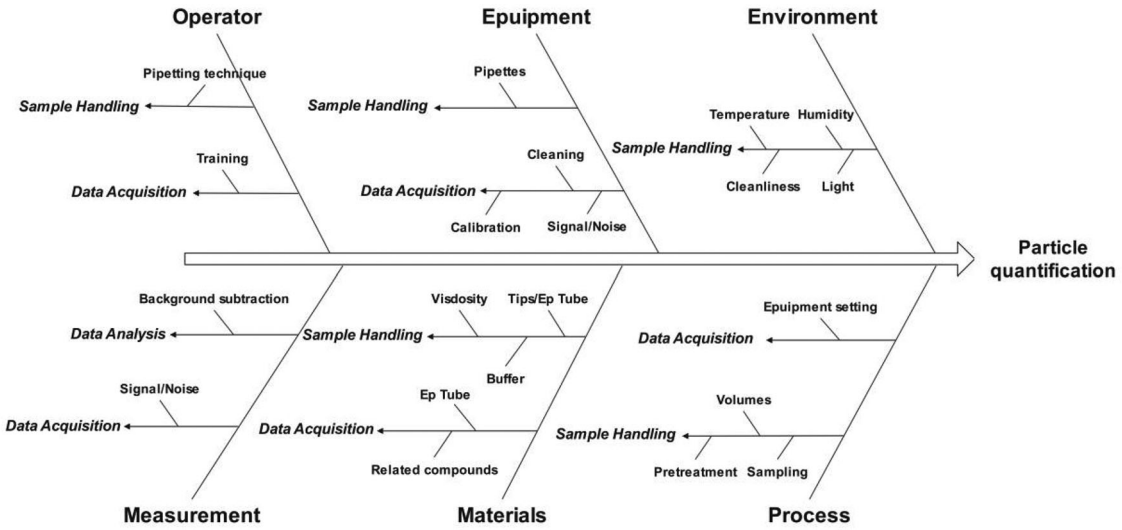

FIGURE 3 | The Ishikawa (fish bone) diagram of risk factor analysis for nanoFCM.

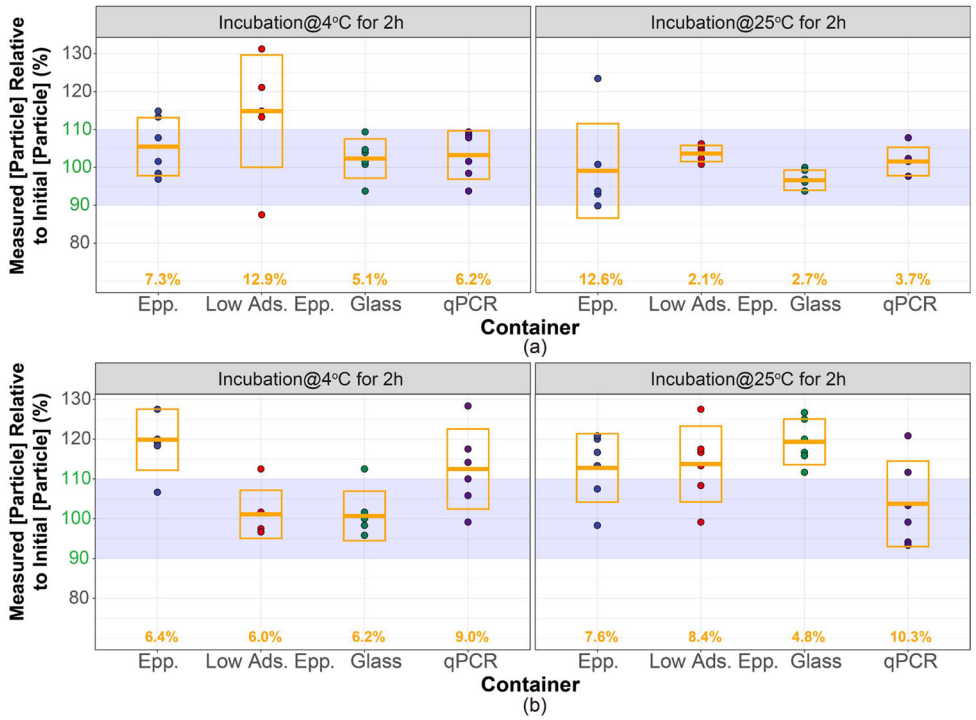

FIGURE 4 | The impact of container on the detection of EVs by nanoFCM. (a and b) Percentage of the detected particle concentration relative to the initial concentration in various tubes for mEVs and hEVs, respectively. The detection was performed after 2 h incubation at 4°C or 25°C. The range between 90% and 110% was highlighted in purple. The types of containers shown on the x-axis include ordinary Eppendorf (Epp.), low adherent Eppendorf (Low Ads. Epp.), glass and qPCR tubes. The orange line and the orange box represent the average value and the RSD of six replicates for each container. The orange numbers on the x-axis indicated the RSD value for each container.

of pipetting during sample dilution. From a 1.5×10^{13} p/mL mEV sample, we produced three batches of 10-fold diluted samples, each subsequently diluted to 1.5×10^{8} p/mL for measurement. Figure 6 shows that a larger volume drawn during dilution was associated with lower measurement variation. When dispensing viscous microliter (μL) solutions, a portion of the solution may stick to the outer surface of the pipette tips, leading to inconsistencies in the actual volume transferred. Higher total volumes turned out to be less susceptible to the impact of adhered sample solution; therefore, it is recommended to aspirate at least 50 μL of concentrated sample to minimise the effects of pipetting errors.

3.3.4 | Process – Sample Dilution

Most EV samples in routine EV R&D require certain degrees of dilution. The optimal range of particle concentration for nanoFCM lies between 10^{7} and 10^{9} p/mL (vide supra), which

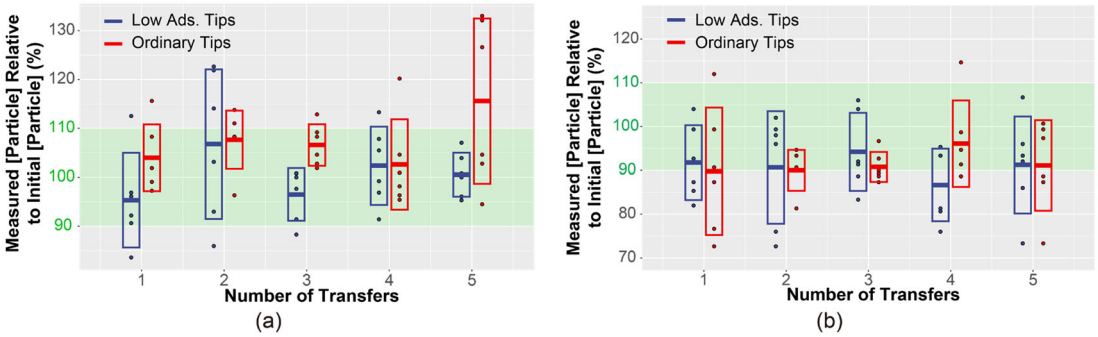

FIGURE 5 | The impact of pipette tips on the detection of EVs by nanoFCM. (a and b) Percentage of the detected particle concentration relative to the initial particle concentration for mEVs and hEVs, respectively. EVs were transferred from the initial tube to five new glass containers sequentially. The number of transfers was shown on the x-axis below. The range between 90% and 110% was highlighted in green. Blue and red dots represent data from the low-adsorption pipette tips group (Low Ads. Tips) and the ordinary pipette tips group (ordinary tips), respectively. In each case, the line in the middle and the box represent the average value and the corresponding RSD value of the six replicates.

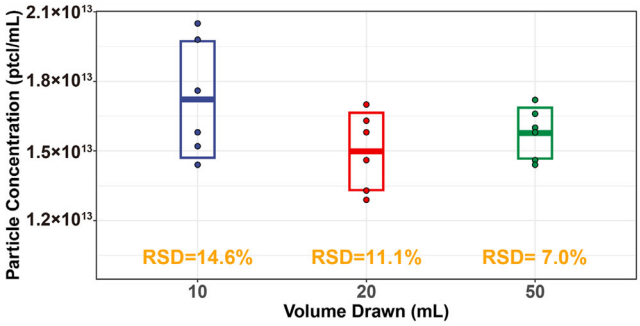

FIGURE 6 | The impact of sampling volume during dilution on nanoFCM detection of mEVs. The original mEV suspension ($\sim 1.5 \times 10^{13}$ p/mL) was sequentially diluted 10-fold for 5 times to $\sim 1.5 \times 10^{8}$ p/mL for nanoFCM analysis. The dilution was performed by mixing 10, 20 or 50 μL of the previous solution with 90, 180 and 450 μL DPBS, respectively, in each step, and the concentrations of the original suspension were calculated and shown as dark blue, red and green dots, respectively. Each sampling volume was done in six replicates. The line in the middle and the box represent the average value and the corresponding RSD value of those six replicates. The RSD values are also shown in the chart.

is often several orders of magnitude lower than the concentrations typically processed during the manufacturing of EV-based therapeutics. Therefore, both in-process testing samples and final products must be adequately diluted to ensure reliable quantification on the nanoFCM. Since the influence of container and pipette tips was already addressed in previous sections, we next hypothesised that the large variation in measurements arose from the propensity for aggregation in the EV population (Evtushenko et al. 2020; Gelibter et al. 2022; Gorgens et al. 2022). To test this hypothesis, we screened a panel of surfactants and additives, known to have an impact on EV stability (Bosch et al. 2016; Osteikoetxea et al. 2015), for their ability of preventing particle aggregation and reducing measurement variation. These include SDS, Triton X-100, Tween 20, Tween 80, sucrose and glycerol (Figure 7a).

Different additives introduced distinctive influences on the measurement outcome. Glycerol did not significantly affect the particle count but reduced variation in hEV samples (Figure 7b,c). Even at extremely low concentrations, SDS skewed the particle count upward, most likely due to the formation of SDS micelles. Sucrose did not affect hEV samples but caused a dose-dependent reduction in particles of mEV samples. The behaviour of Triton X-100 is complex. On one hand, it is known to effectively lyse EV particles at concentrations exceeding 0.1%. On the other hand, Triton X-100 has to be diluted prior to nanoFCM analysis to prevent micelles from being counted as particles. Since Triton X-100 remained undiluted in our assay, we likely observed a combined effect of both EV lysis and micelle formation. Tween-80 again led to a greater alteration in particle counts in mEV than in hEV, whereas Tween-20 did not affect particle counts in either EV type. More importantly, Tween-20 significantly suppressed measurement variation. Known to help preserve EVs (Cimorelli et al. 2021), BSA was also tested at a concentration from 0.1 to 10 mg/mL (Figure S10a). No improvement was observed in reducing the measurement variations, and similar to other proteins, BSA at high concentrations increased the baseline readings of nanoFCM detection (Figure S10b). Thus, it is not suitable for our purpose either.

We further investigated the effect of Tween-20 on improving measurement precision with finer concentration intervals. Figure 7d,e shows that samples containing Tween-20 at approximately 0.03% (w/v) exhibited the lowest variance in particle counts for both mEV and hEV. Owing to the amphiphilic nature and superior hydrophilic-lipophilic balance of Tween-20, in contrast to other tested additives, Tween-20 can adhere to the surface of EVs without compromising their structural integrity and has the least potential to disrupt vesicles (Figure S10c) (Osteikoetxea et al. 2015; Schuck et al. 2003). This observation aligns with multiple earlier independent studies demonstrating that low concentration of Tween-20 EV can preserve EVs' structural integrity(Arab et al. 2021; Islam and Marcus 2024; Osteikoetxea et al. 2015). A reduction in vesicle-vesicle aggregation and vesicle-container adsorption promoted stable mono dispersion of EVs in solution (Figure S10c,d), reducing the variance in particle quantification to acceptable levels.

We further validated this recipe (0.03% w/v Tween-20) in a large number of hEV and mEV samples across a wide range of concentrations (Figure 7f,g). In the absence of Tween-20, higher

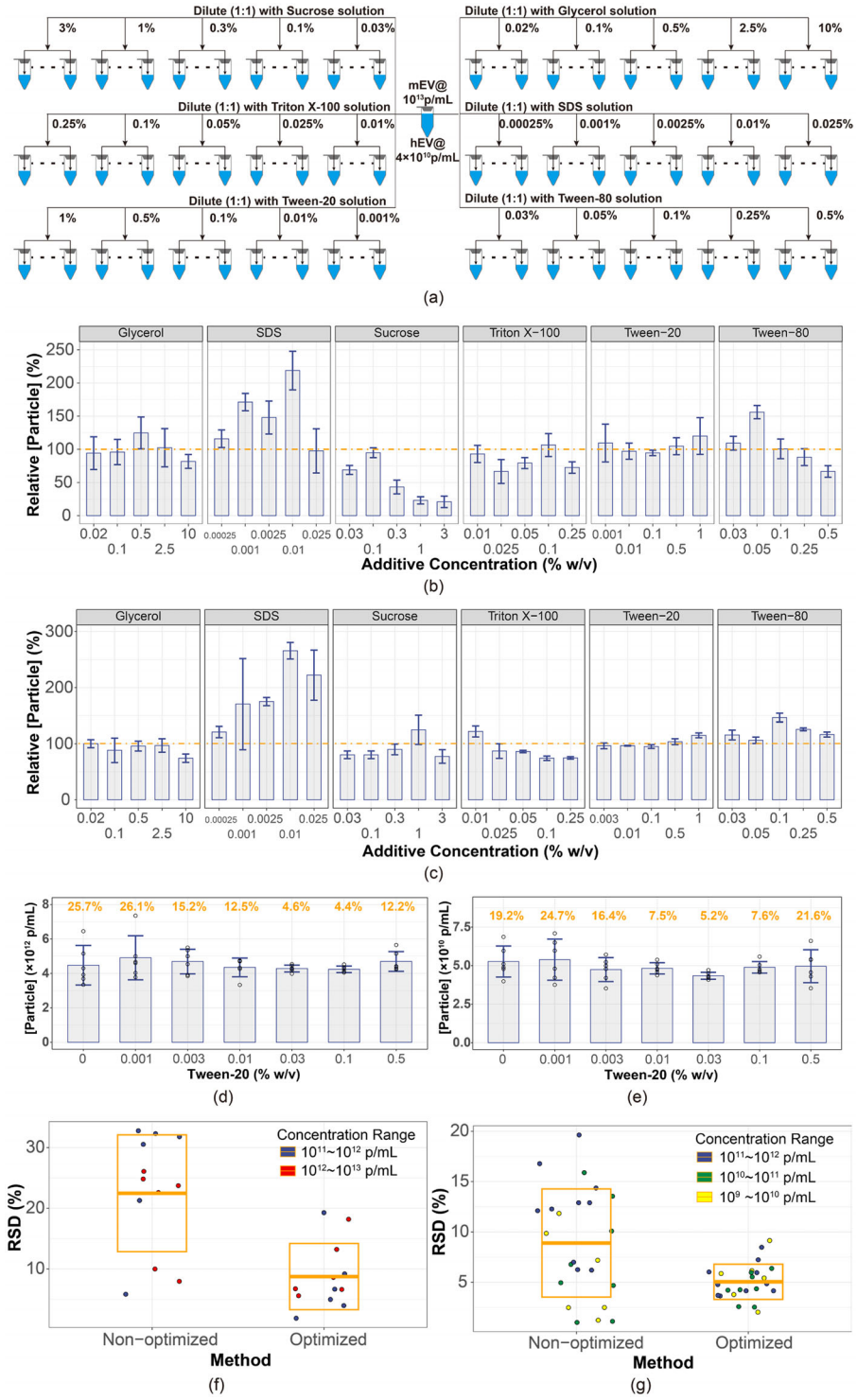

FIGURE 7 | Effects of various dilution reagents on EV counts detected by nanoFCM. (a) experimental procedures of screening types of dispersants. The original EV solutions (mEVs at 1×10^{13} p/mL, hEVs at 4×10^{10} p/mL) were mixed in equal volume with various concentrations of dispersants, including SDS, Triton X-100, Tween-80, Glycerol, Sucrose and Tween-20 (in w/v units except for Glycerol in v/v units). Each concentration of the dispersants was performed in six replicates. All these suspensions were further diluted to the final concentration (1.5×10^{8}–6.0×10^{8} p/mL) before nanoFCM analysis. (b and c) Detected over original particle concentration for mEVs and hEVs, respectively, after dilution with various concentrations of dispersants. The orange line highlighted 100%. The blue error bars represent the standard deviations of each concentration of dispersants. (d and e) The EV particle concentration of the original solution was detected by nanoFCM after pretreatment with Tween-20 at 0.001%, 0.003%, 0.01%, 0.03%, 0.1% and 0.5% for mEVs and hEVs, respectively. The blue error bars and the orange numbers represent the standard deviations and the RSD values with various Tween-20 concentrations shown in the x-axis. (f and g) RSD percentage of the particle counts of mEVs (f) and hEVs (g) detected by nanoFCM without or with the addition of 0.03% Tween-20, respectively (non-optimised and optimised, respectively). The EVs in (f and g) represent various mEVs and hEVs preparations over 6 months in our laboratory. The colour of dots in (f) and (g) indicate concentration ranges of the original mEVs and hEVs samples: 10^{12}–10^{13} p/mL (red), 10^{11}–10^{12} p/mL (blue), 10^{10}–10^{11} p/mL (green), 10^{9}–10^{10} p/mL (yellow).

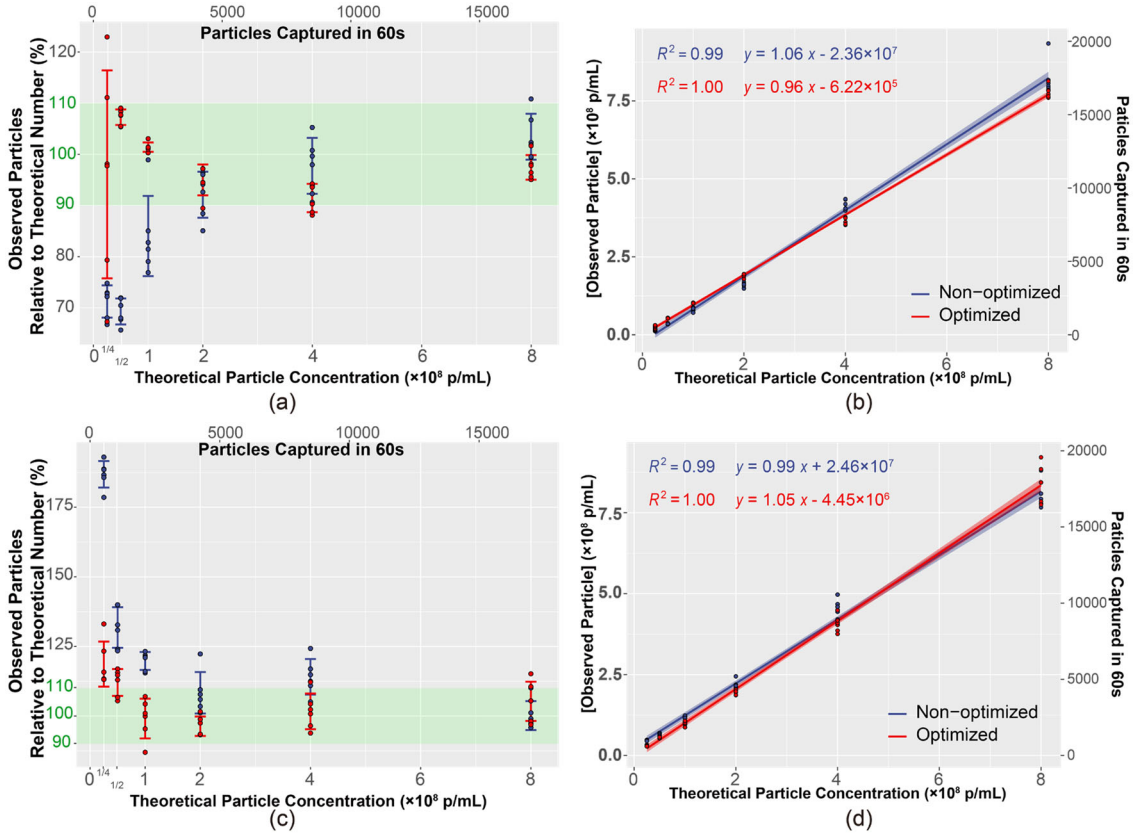

FIGURE 8 | Precision and reportable range of nanoFCM detection for mEVs and hEVs in a serial 2-fold dilution with DPBS and DPBS containing 0.03% Tween-20. The data collected for mEV were presented in (a) and (b), whilst the data collected for hEV were presented in (c) and (d). The particle concentration of the starting solution was ~8×10^8 p/mL. Each dilution was performed in six replicates and analysed by nanoFCM. The blue and red dots showed the concentration of EV suspension without and with 0.03% Tween-20, respectively (non-optimised and optimised, respectively). (a and c) Percentage of observed particle concentration relative to theoretical particle concentration at each theoretical particle concentration for mEVs and hEVs, respectively. The range between 90% and 110% was highlighted in green. The number of particles captured in 60 s was also shown in the x-axis on the top. The RSD values are shown in blue and red bars, respectively, in the chart. (b and d) Regression curves of observed over theoretical particle concentrations for mEVs and hEVs, respectively. The regression equations and the R^2 are also shown in the chart. The number of particles captured in 60 s are shown in the y-axis to the right.

EV concentrations were often associated with higher RSD values, as concentrated EV particles were prone to aggregate (Charoenviriyakul et al. 2018; Kusuma et al. 2018; Trenkenschuh et al. 2022). The presence of Tween-20 successfully suppressed the RSD values to lower levels, independent of the concentration of EV samples. These results, in turn, suggested that the primary source of measurement variation may have been due to uncertainty of aggregation.

3.4 | Re-Evaluation of ATP Characteristics With Optimised Procedure

After adopting the optimised procedure, we carried out an in-depth re-evaluation of the performance characteristics for nanoFCM.

3.4.1 | Accuracy

We observed a comparable improvement in accuracy for both mEV and hEV samples (Figure 8). At concentrations below 1×10^8 p/mL, the measurement variance for hEV samples was slightly better than that for mEV samples, but both met the ±10% accuracy criterion. Method optimisation mitigated the tendency for underestimation and overestimation for mEV and hEV samples, respectively (Figure 8a,c). Another notable outcome of the method optimisation was that the slope of linear regression came closer to 1.00 and the Y-axis intercepts were diminished, suggesting again a significant improvement in accuracy (Figure 8b,d).

3.4.2 | Precision and Reportable Range

Although the plots on a double-log scale appeared nearly identical, the results of linear regression demonstrated substantial improvement of linearity (R^2 increased from 0.91 to 0.99 for mEV and from 0.94 to 1.00 for hEV) and significantly reduced deviation from theoretical/expected values (Figure 9a,c). The slopes dropped below 1.1, and the Y-intercepts were reduced. As shown in Figure 9b,d, only one out of 6 concentration points for mEV and one out of four concentration points for hEV deviated from the theoretical value by more than 10%. More importantly,

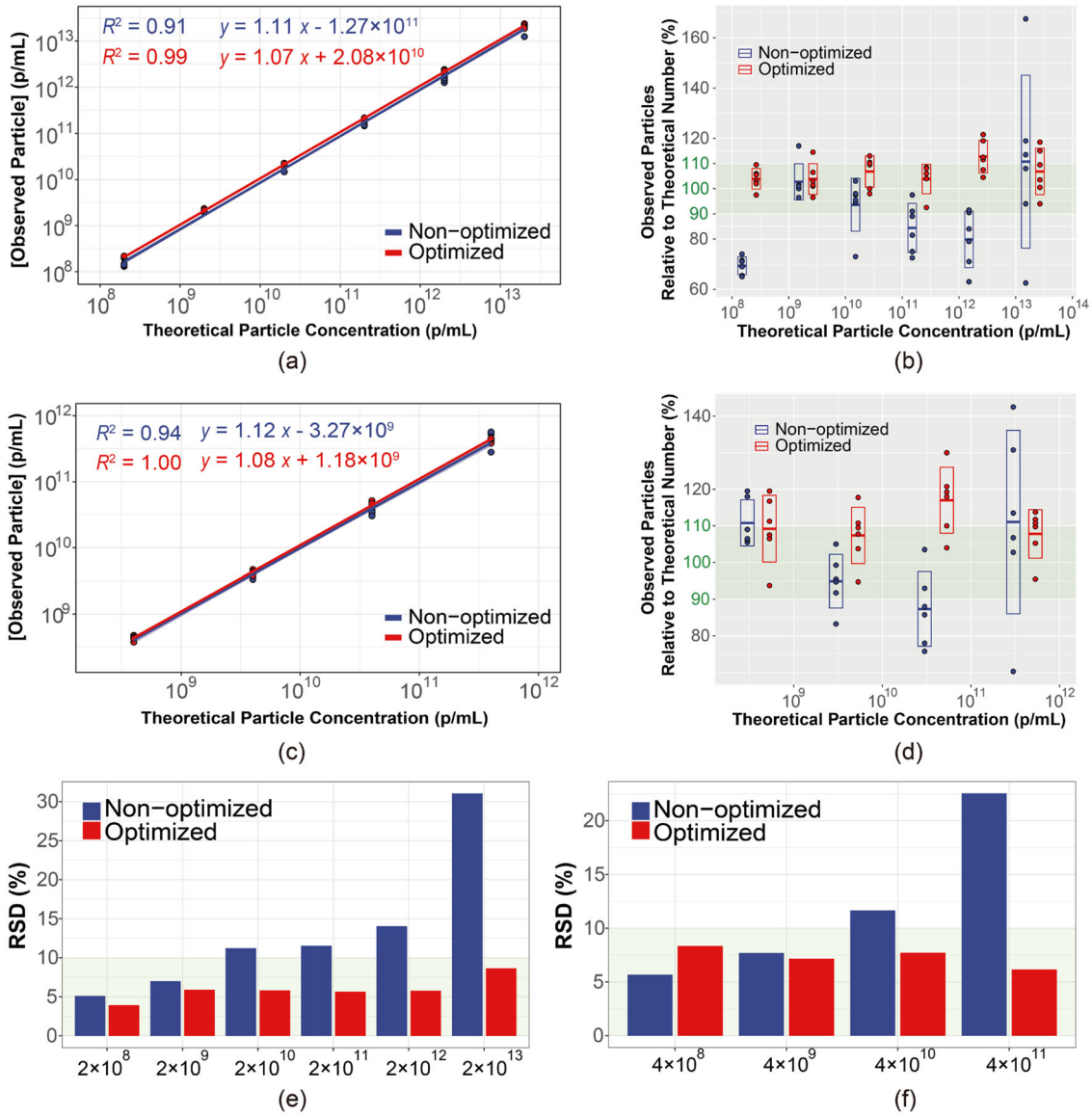

FIGURE 9 | Precision of nanoFCM detection for mEVs and hEVs in a serial 10-fold dilution with DPBS and DPBS containing 0.03% Tween-20. The data collected for mEV were presented in (a), (b) and (e), whilst the data collected for hEV were presented in (c), (d) and (f). The particle concentration of the starting solution was ~2×10^{13} and ~4×10^{11} p/mL for mEVs and hEVs, respectively. Each dilution was performed in six replicates, and all the resulting diluted solutions were analysed by nanoFCM. The blue and red dots showed the experimental data at each theoretical concentration without and with 0.03% Tween-20, respectively (non-optimised and optimised, respectively). (a and c) Regression curves of observed over theoretical particle concentrations for mEVs and hEVs, respectively. The regression equations and the R^2 under non-optimised and optimised conditions were also shown in the charts. (b and d) Percentage of observed particle concentration relative to the theoretical particle concentration at each theoretical particle concentration for mEVs and hEVs, respectively. The range between 90% and 110% was highlighted in green. The line in the middle and the box represent the average value and the corresponding RSD value of the six replicates. (e and f) RSD values of the six replicates at each theoretical particle concentration for mEVs and hEVs, respectively. The 10% threshold is highlighted in green.

the RSD of the optimised procedure no longer depended on the initial particle concentration of the samples or the folds of dilution prior to measurement (Figure 9e,f). It is, therefore, warranted to use a relatively small number of repeats (e.g., 3 vs. 6) during measurements without the risk of obtaining significantly skewed results.

Starting from a 1×10^8 p/mL sample, we carried out serial two-fold dilutions to concentrations as low as 6.25×10^6 p/mL to probe the sensitivity limit of nanoFCM under the optimised conditions. Figure 10a–d demonstrate that the precision criteria were met at 5×10^7 p/mL, below which the measurement variance exceeded the 10% threshold. The particle number can be accurately determined at 1.25×10^7 p/mL despite the increased variance. However, the instrument was unable to accurately measure the concentration of the 6.25×10^6 p/mL samples for either mEV or hEV (Figure 10e,f).

Combining the results from our accuracy evaluation, the linear range of nanoFCM for mEV is from 5×10^7 p/mL (LLOQ) to

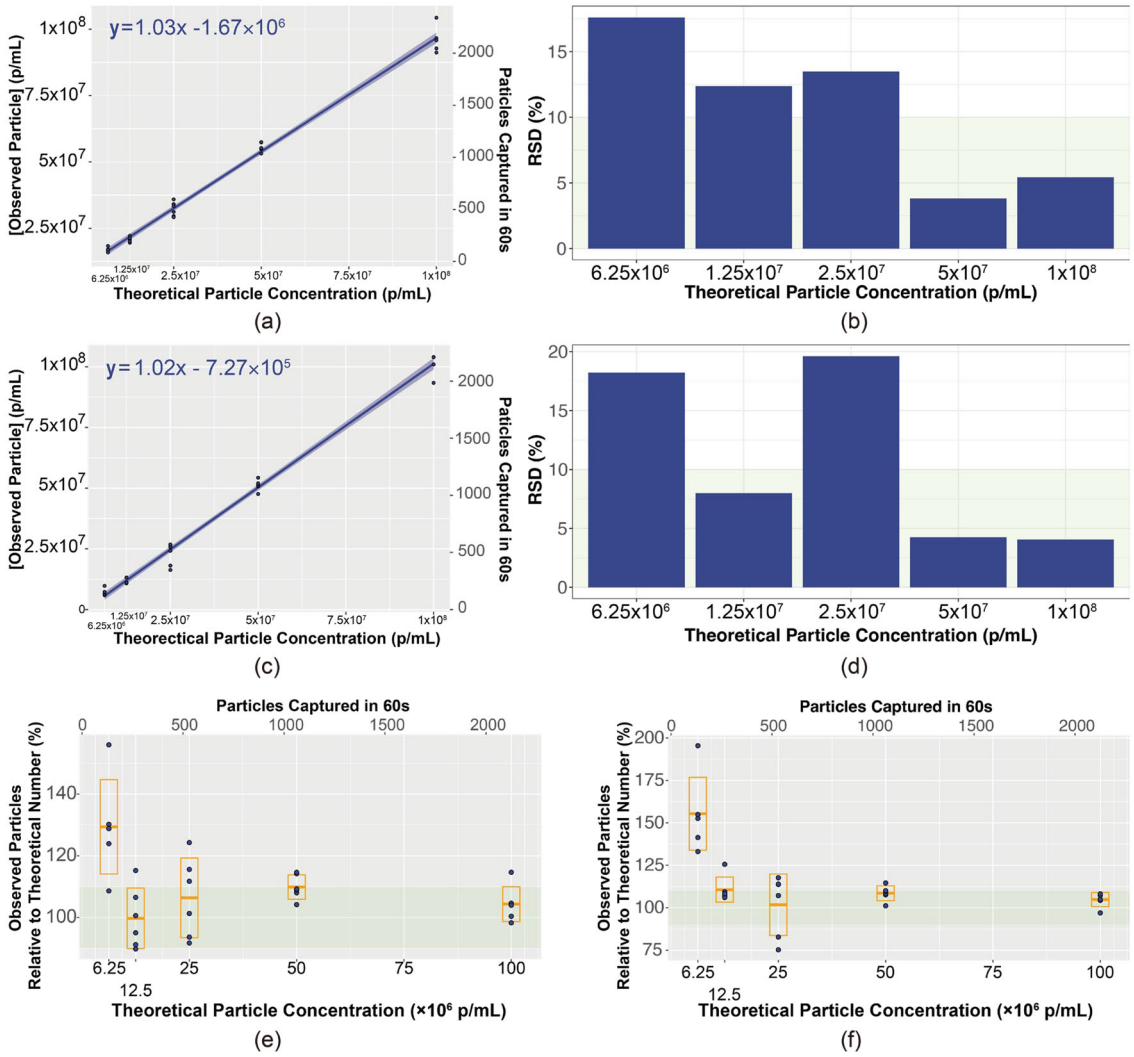

FIGURE 10 | Reportable range of nanoFCM detection for mEVs and hEVs in a serial 2-fold dilution with DPBS containing 0.03% Tween-20. The data collected for mEV were presented in (a), (b) and (e), whilst the data collected for hEV were presented in (c), (d) and (f). The particle concentration of the starting solutions for mEVs and hEVs was 1.0×10^8 p/mL. Each dilution was performed in six replicates, and all the resulting diluted solutions were analysed by nanoFCM. (a and c) Regression curves of observed particle concentrations over theoretical particle concentrations for mEVs and hEVs, respectively. The regression equation was also shown in the charts. (b and d) RSD values of the six replicates at each theoretical particle concentration for mEVs and hEVs, respectively. The 10% threshold is highlighted in green. (e and f) Percentage of observed particle concentration relative to the theoretical particle concentration at each theoretical particle concentration for mEVs and hEVs, respectively. The number of particles captured in 60 s are also shown in the x-axis at the top. The orange line in the middle and the orange box represent the average value and the corresponding RSD value of the six replicates in the nanoFCM detection results. The range between 90% and 110% was highlighted in green.

2×10^{13} p/mL (ULOQ), with an LOD of 2.5×10^7 p/mL. For hEV, the linear range of nanoFCM measurement is from 1×10^8 p/mL(LLOQ) to 4×10^{11} p/mL (ULOQ), with an LOD of 1×10^8 p/mL.

3.4.3 | Robustness

3.4.3.1 | Non-Particulate Impurities. We investigated the impact of common biomolecular impurities on particle quantification, with mEV and hEV samples of predetermined concentration (8×10^8 p/mL). In general, the presence of non-particulate impurities did not impair the precision of the measurement (Figure 11a,d), as the RSD values were mostly within an acceptable range, except at elevated concentrations. For the 29 kDa protein (Carbonic Anhydrase), there was a clear trend of increasing number of detected particles with a rising protein concentration, manifested as greater deviation from the Blank sample concentration (Figure 11b). Beyond 40 μg/mL, the deviation in particle count exceeded the acceptable range, along with a substantial shift in the signal baseline (Figure 11c). For the 158 kDa protein (Aldolase), the nanoFCM instrument could tolerate up to 400 ug/mL for mEV and 4 mg/mL for hEV without deviating from the acceptable range in both particle number and signal baseline (Figure 11b, c, e,f). However, for the 669 kDa protein (Thyroglobulin), even at low concentrations, its presence skewed the measurement outcome. Proteins can give rise to 'ghost' particle signals when they aggregate into large nanoparticles at elevated concentrations, skewing the particle count upward. In addition, a high concentration of free protein

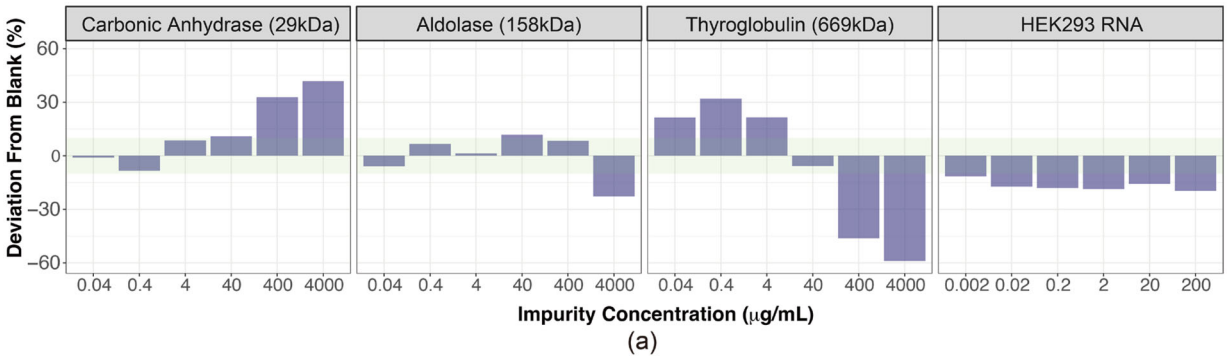

(a)

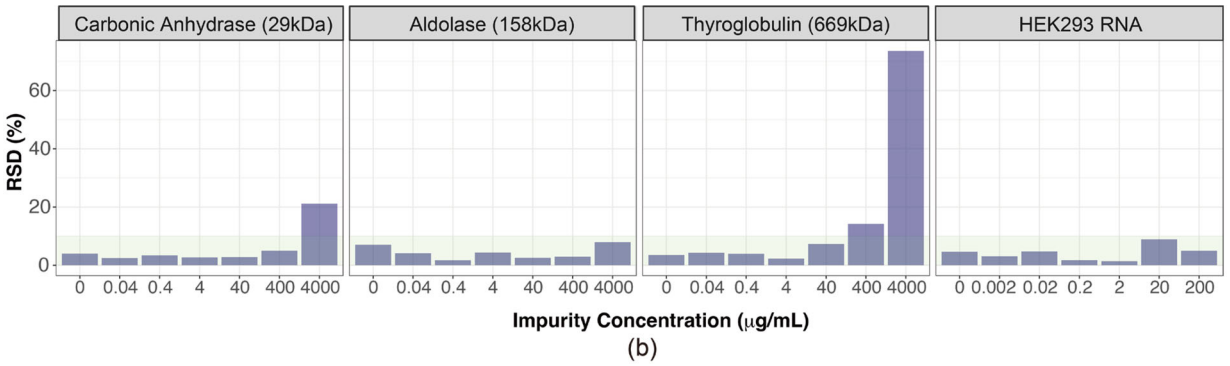

(b)

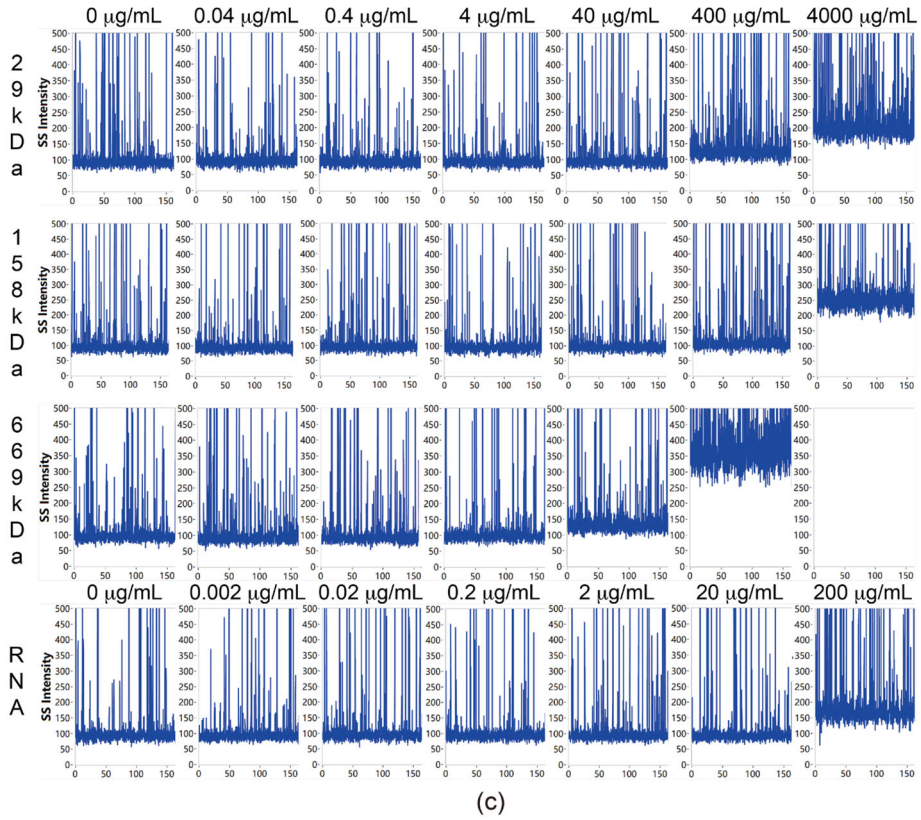

(c)

FIGURE 11 | Effects of non-particulate impurities on EVs concentration detection by nanoFCM. Standard solutions of mEVs and hEVs (8×10^8 p/mL) were analysed by nanoFCM after mixing 1:1 with various levels of non-particular impurities, including carbonic anhydrase (29 kDa), aldolase (158 kDa), thyroglobulin (669 kDa) and total RNA from HEK293F cells. (a and d) Deviation of the concentration of EVs containing non-particulate impurities from the concentration of EVs without those impurities for mEVs and hEVs, respectively. The range between -10% and 10% was highlighted in green. (b and e) The RSD values of the six replicates at each concentration of non-particulate impurities for mEVs and hEVs, respectively. The 10% threshold is highlighted in green. (c and f) SS-Intensity (side scatter intensity) over SSC (side scatter channel) during the nanoFCM detection of EVs with various concentrations of non-particulate impurities for mEVs and hEVs, respectively.

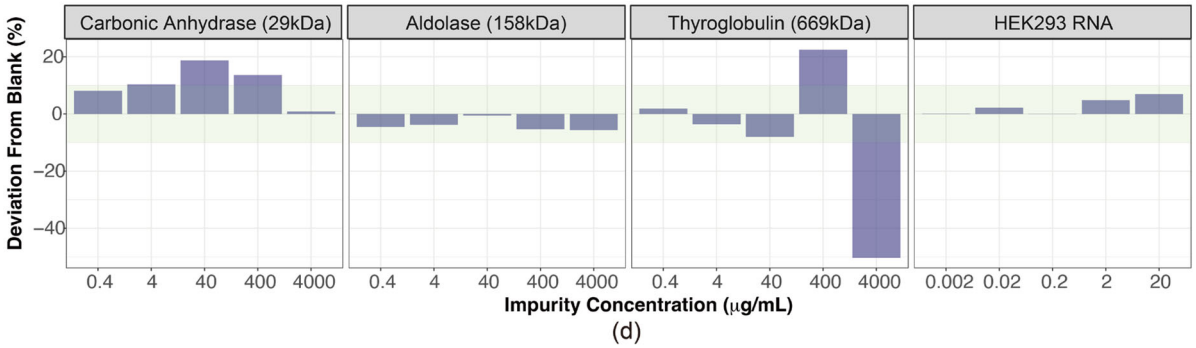

(d)

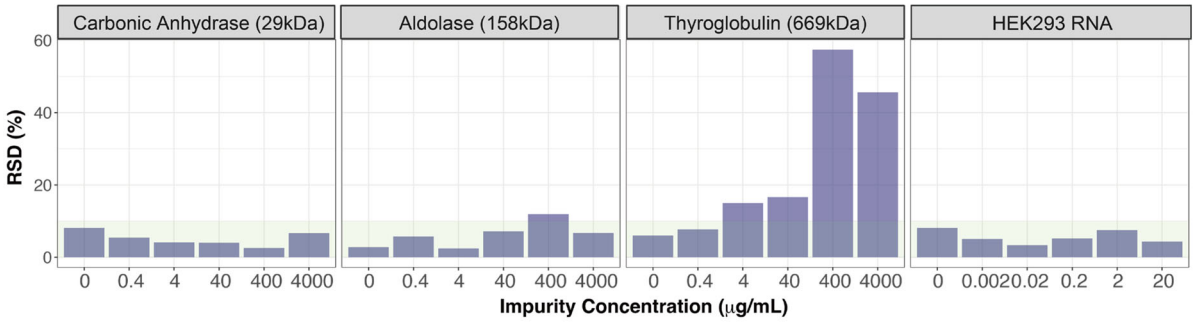

(e)

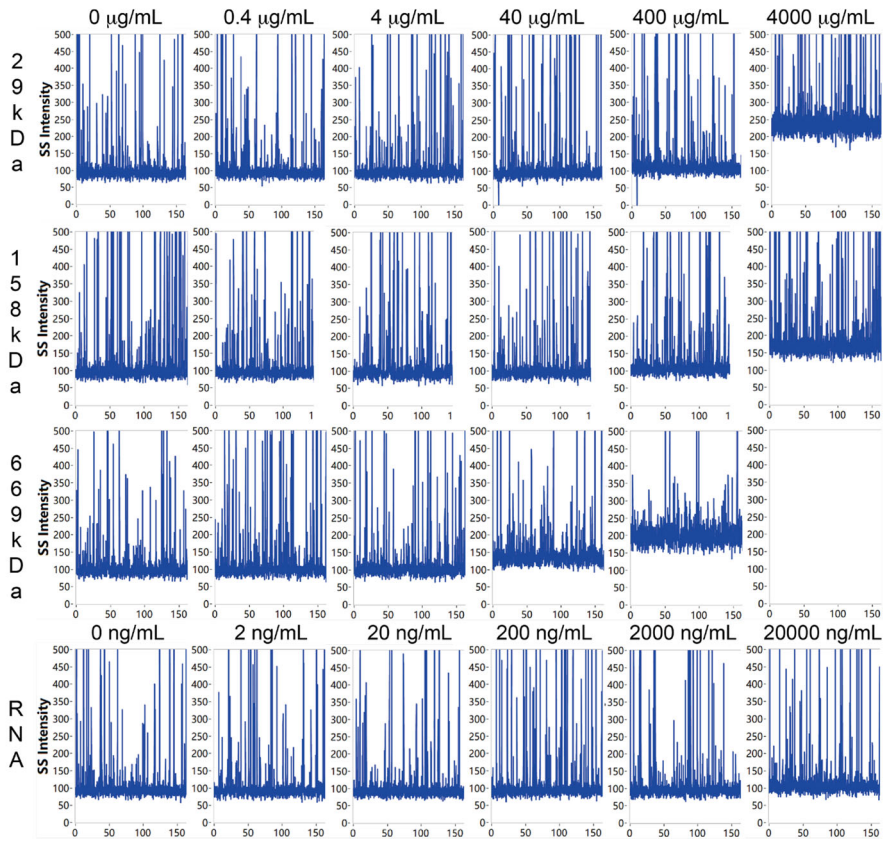

(f)

FIGURE 11 | (Continued)

elevates the signal baseline (Figure S11), potentially masking signals from genuine EV particles and hence leading to an underestimation of particle number. These two counteracting effects gave rise to the observed non-monotonic trend in particle numbers. Since most naturally occurring proteins have molecular weights of less than 200 kDa, it might be appropriate to allow free protein with a concentration of up to 40 μg /mL, whilst remaining vigilant with large, aggregation-prone protein. The presence of genomic RNA fragments, a common impurity in cell-derived EV products, caused the particle number of mEVs to skew

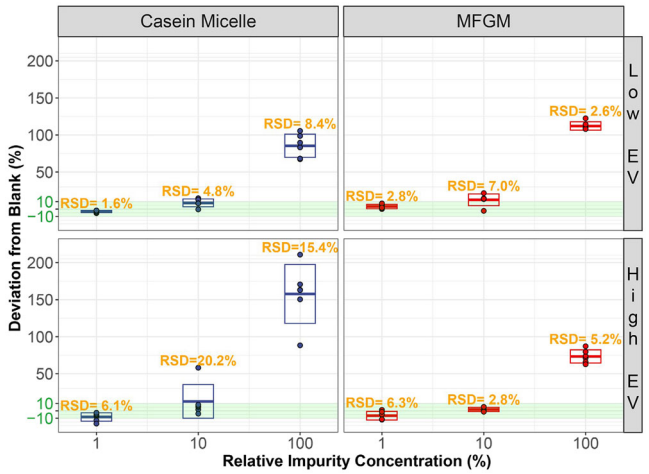

FIGURE 12 | Effects of particulate impurities casein micelle and MFGM on mEV concentration detection by nanoFCM. Milk EV was used in this assay at low and high concentrations (4×10^8 and 4×10^{11} p/mL, respectively). Casein micelle and MFGM were present at 1%, 10% and 100% relative to the concentrations of the mEV stock solutions. Deviation of the concentration of mEVs containing various levels of particulate impurities from the concentration of mEVs without those impurities (designated Blank) was shown. The range between −10% and 10% deviation was highlighted in green. The lines in the middle of the box and the box represent the average value and the corresponding standard deviation of the six replicates in the nanoFCM detection results. Also shown in the chart were the RSD values.

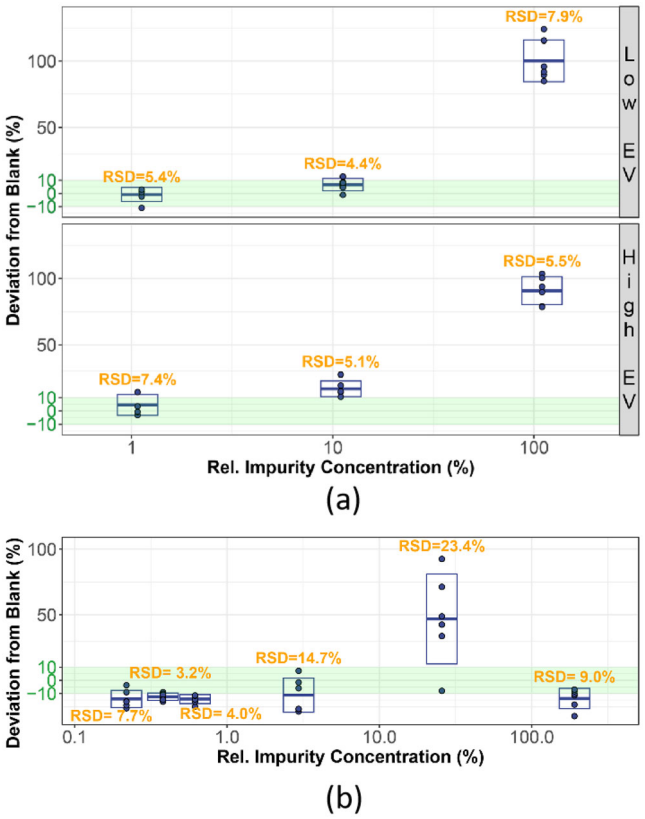

FIGURE 13 | Effects of particulate impurities, cellular debris and DNA fragment on hEV concentration detection by nanoFCM. (a) Deviation of the concentration of hEVs containing various levels of cellular debris from the concentration of hEVs without those impurities (designated Blank) was shown. HEK293 EV was used in this assay at low and high concentrations (4×10^8 and 4×10^{10} p/mL, respectively). Cellular debris was present at 1%, 10% and 100% relative to the concentrations of the hEV stock solutions. (b) Deviation of the concentration of hEVs containing various levels of DNA fragments from the concentration of hEVs without those impurities (designated Blank) was shown. HEK293 EV was used in this assay at 8×10^8 p/mL. DNA fragment was present at 0.3%, 0.5%, 0.7%, 3.6%, 30.1% and 230.1% relative to the concentrations of the hEV stock solution. The range between -10% and 10% deviation was highlighted in green. The lines in the middle of the box and the box represent the average value and the corresponding RSD value of the six replicates in the nanoFCM detection results. Also shown in the chart were the RSD values.

downward at concentrations as low as 20 ng/mL for unknown reasons (Figure 11a,b). In contrast, hEV products were found to be much more tolerable to HEK293 cell-derived RNAs (Figure 11d,e).

3.4.3.2 | Particulate Impurities.

a. Casein Micelles and MFGM

Casein micelles and MFGM are the two major particulate impurities in mEV. Our results showed that the relative population of casein micelle and MFGM to mEV was more pertinent to measurement outcome than their absolute concentration (Figure 12). Casein, the primary protein component in milk, becomes indistinguishable from EVs on nanoFCM upon formation of micelle and were thus quantified as particles when they account for more than 10% of the total particulate matter (Figure 12). Casein micelles possess a unique feature of reversible aggregation and disaggregation, which may introduce random errors when present at high concentrations (De 2014; Horne 2020). Indeed, when the concentration of casein micelles exceeded 2×10^{10} p/mL, in addition to a significant deviation from the expected particle number, the RSD of the nanoFCM measurement rose above the 10% acceptable limit.

MFGM is abundant in a variety of dairy products. NanoFCM analysis of EV samples spiked in with MFGM ($\varnothing \leq 450$ nm) showed that nanoFCM could not distinguish between EVs and MFGM. Thus, if the content of MFGM exceeds 10% of EV particles, the accuracy of the measurement will be significantly impaired (Figure 12). However, unlike casein micelles, the presence of MFGM did not affect the precision of the measurement, as the RSDs consistently remained well below 10%.

b. Cellular Debris and Large DNA Fragment

For hEV, we investigated the impact from cellular debris (sonicated HEK293F cells) and large DNA fragments (DNA plasmid). The effect of cellular debris was more predictable compared to DNA fragment, as the deviation from Blank (level of accuracy) depended upon the impurity population relative to hEV (Figure 13). In addition, the RSD (level of precision) consistently remained below 10% regardless of the absolute and relative

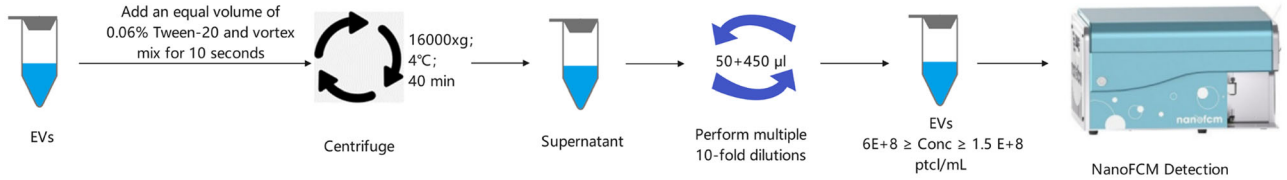

FIGURE 14 | An optimised procedure for the enumeration of particles using nanoFCM. The EV concentration detection process, following the optimisation of the particle concentration detection method on nanoFCM, involves the following steps: The EV stock solution was 1:1 mixed with DPBS containing 0.06% Tween-20 and then centrifuged at 16,000 × *g* at 4°C for 40 min. After centrifugation, the supernatant of EVs was collected and subjected to serial dilutions (up to 10-fold per dilution: 50 + 450 µL) until the concentration reached the range of 6.0×10^8 to 1.5×10^8 p/mL. The particle concentration was measured using nanoFCM.

concentrations of the impurity. For DNA plasmid, however, even if it was difficult to reach a high level of particle concentration with DNA fragment, its negative impact on both the accuracy and precision of measurement was evident with great uncertainty in regard to their relative concentration (Figure 13).

4 | Discussion

The quantification of particle numbers is arguably the most important analytical procedure for EV-based therapeutics. It is so routinely conducted that little attention is paid to the performance characteristics of the operating procedure. Among the many capabilities of nanoFCM, particle number quantification is the most frequently performed procedure. The recently released ICH Q14 guideline allowed us to revisit the analytic procedure of nanoFCM systematically. We provided an optimised protocol for measuring the particle concentration of EV samples using the nanoFCM instrument (Figure 14).

Precision is relatively the most poorly optimised aspect of the nanoFCM procedure, as it received the least attention in previous studies. From our evaluation and optimisation, it is evident that the mean outcome from a nanoFCM measurement is generally reliable, even without optimisation, provided that an adequate number of repeats is used ($n \geq 6$). However, this is not always guaranteed. Our results showed that the large RSD associated with a non-optimised procedure would render a typical $n = 3$ measurement unreliable. Even after adopting the optimised procedure, special care is recommended when dealing with samples out of the optimal range (i.e., $< 10^8$ or $> 10^{12}$ p/mL).

NanoFCM does not typically detect proteins and oligonucleotides as particles. Therefore, non-particulate impurities, in principle, do not interfere with the quantification of particles. For EV-based therapeutics (mEV, hEV, as well as other types of EVs or nanovesicles harvested from cell culture), free proteins constitute the primary impurities from both quality and safety perspectives. Our study showed that proteins smaller than 200 kDa may be of limited impact on nanoFCM measurement, except at elevated concentrations. However, large proteins with diameters approaching those of nanoparticles could skew nanoFCM measurements, even at low concentrations. A particularly relevant scenario is in-process testing of cell culture supernatant or cell extrusion suspension, where myriad free proteins may be present at substantial levels, potentially leading to significant baseline shifts. A sample pretreatment procedure (possibly involving ultracentrifugation) is thus necessary to reliably enumerate the vesicles in these samples.

Particulate impurities are often indistinguishable from EV particles on nanoFCM. Their interference to measurements depends more on their abundance relative to EV particles, rather than their absolute concentration. MFGM and cellular debris ($\varnothing \leq 450$ nm), due to their structural stability, did not increase uncertainty in the measurement. However, casein micelles and DNA fragments introduced significant interference, likely because of their reversible and dynamic transitions among various aggregation/folding states. Specific sample pretreatment methods are required for the instrument to distinguish among different types of nanoscale particles or fragments, which is beyond the scope of this study.

5 | Conclusion

NanoFCM is a powerful and reliable instrument, offering precise and accurate particle quantification across a concentration range spanning 6 orders of magnitude. The complete ATP for nanoFCM, developed as one of the key outcomes of this study, is laid out below:

Analytical target profile (ATP) of nanoFlow cytometry (nanoFCM)

Intended purpose

To quantify the number of EV particles in a given volume within a given sample, thereby deducing the particle concentration in this sample.

Link to CQA

The number (concentration) of EV particles is a prerequisite for a number of critical procedures in the manufacturing process: (1) API loading; (2) filling amount in the final formulation. The number of particles is a vital factor for the delivery capacity of the final formulation, which predicates safety and efficacy.

Characteristics of the reportable result

Performance characteristics	Acceptance criteria	Rationale
Accuracy	−10.0% ≤ deviation from theoretical particle number ≤10.0%	Due to a lack of standard EV particles with independently quantified particle numbers, a two-fold dilution approach is used for determining the accuracy of measurement (with expected particle concentration below 10^9 p/mL): the deviation of the measured particle number from the theoretical particle number must not exceed ±10%.
Precision	RSD < 10%	Under optimised procedure, within the established concentration range (determined on a product-dependent basis), for an adequately purified sample, the relative variation (RSD) among certain number of repeated measurements (e.g., 6 repeats) should be within 10%.
Robustness	Non-particulate impurities: Nucleic acid ≤ 20ug/mL 29 kDa protein ≤ 40ug/mL 158 kDa protein ≤ 400ug/mL 669 kDa protein ≤ 40 ng/mL Particulate impurities: MFGM≤10% of EV ps Casein micelle≤1% of EV ps Cellular debris ≤ 10% of EV & ≤ 10^9p/mL Large DNA fragments ~ ND	NanoFCM measurement is susceptible to the impact of various types of impurities. The reliability of measurement for upstream samples can be doubtful in the presence of various amounts of certain impurities. Note: The investigation of impurities that are relevant to the EV-based product should be prioritised.
Reportable range	mEV: LOD: $2.5 \times 10^{7\,\#}$ LLOQ: 5×10^7 ULOQ (without dilution): 8×10^8 ULOQ (with dilution): 2×10^{13} hEV: LOD: $1 \times 10^{8\,\#}$ LLOQ: 1×10^8 ULOQ (without dilution): 8×10^8 ULOQ (with dilution): 4×10^{11} *	#: LOD is susceptible to the presence of intrinsic particulate species in the solvent. Using solvent with a priori removal of particulate impurities might improve LOD to lower levels. Current values reflect the LOD achieved with ordinary PBS solvent commercially available. *: ULOQ of hEV is subjected to exploration with higher quantities of samples.

Finally, we hope this study serves as a primer for future studies, in which all major analytical procedures in the EV field can undergo ICH-Q14-guided evaluation and optimisation in order to fortify the methodological foundation of EV-based therapeutics.

Author Contributions

Ganghui Li: Data curation; investigation; methodology; validation; writing - review and editing. **Qizhe Cai**: Conceptualization; data curation; investigation; methodology; project administration; supervision; writing - review and editing. **Yanan Dong**: Methodology; project administration; resources; validation. **Xiang Li**: Methodology; resources; validation; writing - review and editing. **Xi Qin**: Conceptualization; methodology; resources; validation; writing - review and editing. **Miaomiao Xue**: Investigation; resources; writing - review and editing. **Haifeng Song**: Funding acquisition; project administration; resources; writing - review and editing. **Yi Wang**: Conceptualization; data curation; formal analysis; investigation; methodology; project administration; software; supervision; visualization; writing - original draft; writing - review and editing.

Acknowledgments

We thank Mr. Zhu Yang of EVhance Co Ltd. for the insightful discussion and technical support during the EV sample preparation.

Conflicts of Interest

Dr. Yi Wang is the founder and CEO of PanExo Biotech Co. Ltd. Ms. Yanan Dong and Dr. Miaomiao Xue are employees of PanExo Biotech Co. Ltd. The other authors declare no conflicts of interest.

Data Availability Statement

The data that supports the findings of this study are available in the supplementary material of this article

References

Arab, T., E. R. Mallick, Y. Y. Huang, et al. 2021. "Characterization of Extracellular Vesicles and Synthetic Nanoparticles With Four Orthogonal Single-Particle Analysis Platforms." *Journal of Extracellular Vesicles* 10, no. 6: e12079. https://doi.org/10.1002/jev2.12079.

Bosch, S., L. de Beaurepaire, M. Allard, et al. 2016. "Trehalose Prevents Aggregation of Exosomes and Cryodamage." *Scientific Reports* 6: 36162. https://doi.org/10.1038/srep36162.

Charoenviriyakul, C., Y. Takahashi, M. Morishita, M. Nishikawa, and Y. Takakura. 2018. "Role of Extracellular Vesicle Surface Proteins in the Pharmacokinetics of Extracellular Vesicles." *Molecular Pharmaceutics* 15, no. 3: 1073–1080. https://doi.org/10.1021/acs.molpharmaceut.7b00950.

Cimorelli, M., R. Nieuwland, Z. Varga, and E. van der Pol. 2021. "Standardized Procedure to Measure the Size Distribution of Extracellular Vesicles Together With Other Particles in Biofluids With Microfluidic Resistive Pulse Sensing." *PLoS ONE* 16, no. 4: e0249603.

De, C. 2014. "The Structure of Casein Micelles: A Review of Small-angle Scattering Data." *Journal of Applied Crystallography* 47, no. 5: 1479–1489. https://doi.org/10.1107/S1600576714014563.

Evtushenko, E. G., D. V. Bagrov, V. N. Lazarev, M. A. Livshits, and E. Khomyakova. 2020. "Adsorption of Extracellular Vesicles Onto the Tube Walls During Storage in Solution." *PLoS ONE* 15, no. 12: e0243738. https://doi.org/10.1371/journal.pone.0243738.

Gelibter, S., G. Marostica, A. Mandelli, et al. 2022. "The Impact of Storage on Extracellular Vesicles: A Systematic Study." *Journal of Extracellular Vesicles* 11, no. 2: e12162. https://doi.org/10.1002/jev2.12162.

Gorgens, A., G. Corso, D. W. Hagey, et al. 2022. "Identification of Storage Conditions Stabilizing Extracellular Vesicles Preparations." *Journal of Extracellular Vesicles* 11, no. 6: e12238. https://doi.org/10.1002/jev2.12238.

Horne, D. S. 2020. "Chapter 6 - Casein micelle Structure and stability." In *Milk Proteins* 3rd ed., edited by M. Boland and H. Singh, 213–250. Academic Press. https://doi.org/10.1016/B978-0-12-815251-5.00006-2.

International Council for Harmonisation of Technical Requirements for Pharmaceuticals for Human Use. 2023. ICH guideline Q14 on analytical procedure development and validation. https://database.ich.org/sites/default/files.

Islam, M. K. B., and R. K. Marcus. 2024. "Isolation and Quantification of Human Urinary Exosomes Using a Tween-20 Elution Solvent From Polyester, Capillary-Channeled Polymer Fiber Columns." *Analytica Chimica Acta* 1329: 343242.

Kusuma, G. D., M. Barabadi, J. L. Tan, D. A. V. Morton, J. E. Frith, and R. Lim. 2018. "To Protect and to Preserve: Novel Preservation Strategies for Extracellular Vesicles." *Frontiers in pharmacology* 9: 1199. https://doi.org/10.3389/fphar.2018.01199.

Leung, J., D. Pollalis, G. K. G. Nair, et al. 2024. "Isolation and Characterization of Extracellular Vesicles Through Orthogonal Approaches for the Development of Intraocular EV Therapy." *Investigative Ophthalmology & Visual Science* 65, no. 3: 6. https://doi.org/10.1167/iovs.65.3.6.

Mladenovic, D., J. Brealey, B. Peacock, K. Kroot, and N. Zarovni. 2025. "Quantitative Fluorescent Nanoparticle Tracking Analysis and Nano-Flow Cytometry Enable Advanced Characterization of Single Extracellular Vesicles." *J. Extracell Biol.*, 4, no. 1: e70031.

Osteikoetxea, X., B. Sodar, A. Nemeth, et al. 2015. "Differential Detergent Sensitivity of Extracellular Vesicle Subpopulations." *Organic & Biomolecular Chemistry* 13, no. 38: 9775–9782. https://doi.org/10.1039/c5ob01451d.

Sadiq, U., H. Gill, and J. Chandrapala. 2021. "Casein Micelles as an Emerging Delivery System for Bioactive Food Components." *Foods* 10, no. 8: 1965. https://doi.org/10.3390/foods10081965.

Schuck, S., M. Honsho, K. Ekroos, A. Shevchenko, and K. Simons. 2003. "Resistance of Cell Membranes to Different Detergents." *Proceedings of the National Academy of Sciences of the United States of America* 100, no. 10: 5795–5800. https://doi.org/10.1073/pnas.0631579100.

Tian, Y., M. Gong, Y. Hu, et al. 2020. "Quality and Efficiency Assessment of Six Extracellular Vesicle Isolation Methods by Nano-Flow Cytometry." *Journal of Extracellular Vesicles* 9, no. 1: 1697028. https://doi.org/10.1080/20013078.2019.1697028.

Trenkenschuh, E., M. Richter, E. Heinrich, M. Koch, G. Fuhrmann, and W. Friess. 2022. "Enhancing the Stabilization Potential of Lyophilization for Extracellular Vesicles." *Advanced Healthcare Materials* 11, no. 5: e2100538. https://doi.org/10.1002/adhm.202100538.

Xu, M., G. Chen, Y. Dong, et al. 2022. "Liraglutide-Loaded Milk Exosomes Lower Blood Glucose When Given by Sublingual Route." *Chemmedchem* 17, no. 10: e202100758. https://doi.org/10.1002/cmdc.202100758.

Yim, K. H. W., O. Krzyzaniak, A. a. Al Hrout, B. Peacock, and R. Chahwan. 2023. "Assessing Extracellular Vesicles in Human Biofluids Using Flow-Based Analyzers." *Advanced Healthcare Materials* 12, no. 32: 2301706.

Supporting Information

Additional supporting information can be found online in the Supporting Information section.